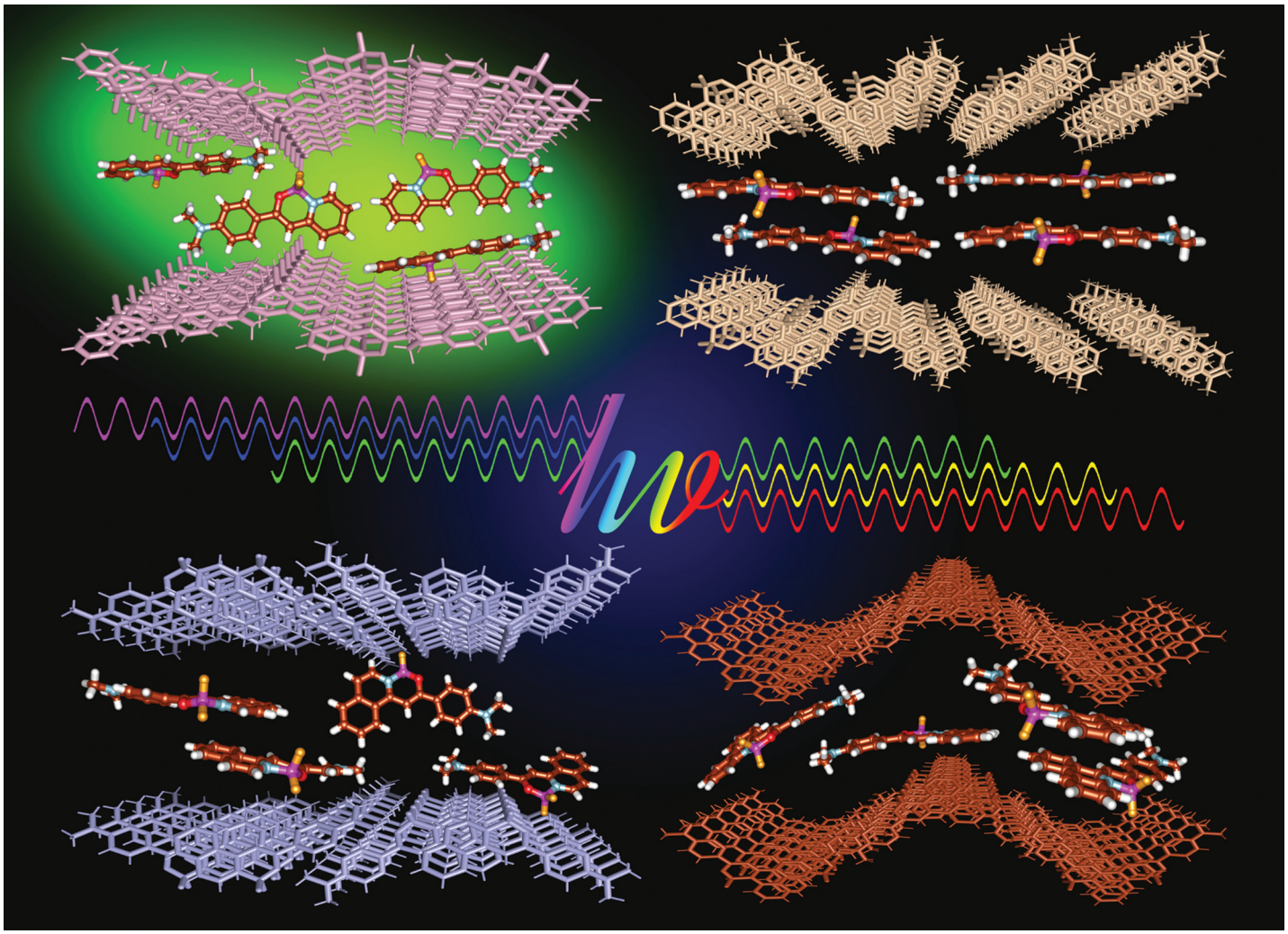

Showcasing research from Nicolaus Copernicus University, Toruń, Poland, performed in collaboration with European laboratories.

Less is more: on the effect of benzannulation on the solid-state emission of difluoroborates

In this work, the design strategy for the preparation of crystals of highly emissive donor–acceptor-substituted fluorescent dyes is revisited. CH $\cdots\pi$ intermolecular interactions between a strong electron-donating $N(CH_3)_2$ group and fused benzo rings are shown to have detrimental effect on the emission properties.

As featured in:

See Denis Jacquemin, Borys Ośmiałowski, Robert Zaleśny *et al.*, *J. Mater. Chem. C*, 2021, **9**, 15820.

ROYAL SOCIETY OF CHEMISTRY

rsc.li/materials-c

Registered charity number: 207890

Journal of Materials Chemistry C

ROYAL SOCIETY OF CHEMISTRY

PAPER

View Article Online
View Journal | View Issue

Cite this: J. Mater. Chem. C, 2021, 9, 15820

Less is more: on the effect of benzannulation on the solid-state emission of difluoroborates†

Iryna Knysh, [a] Anna Kozakiewicz-Piekarz, [b] Andrzej Wojtczak, [b] Damian Plażuk, [c] Glib Baryshnikov, [de] Rashid Valiev, [fg] Rinat Nasibullin, [f] Hans Ågren, [h] Denis Jacquemin, *[i] Borys Ośmiałowski *[b] and Robert Zaleśny *[a]

We investigate the emission properties of four organic dyes containing a strong electron-donating $N(CH_3)_2$ group and an NBF_2O-bearing heterocyclic moiety acting as the electron-accepting group. The four studied compounds differ in the number and positions of the fused benzo rings included in the heterocyclic moiety. They exhibit strong emission in solution, with fluorescence quantum yields (Φ_f) systematically exceeding 0.8 at least in one of the solvents used, regardless of the benzannulation architecture. The strong dipolar character, achieved by substitution with the $N(CH_3)_2$ group and benzannulation, enhances the photoinduced charge transfer and appears to be an effective strategy to tune the photophysical properties of these dyes in solution. Indeed, red-shifted absorption spectra are obtained without deteriorating the emission properties. However, the present joint theory–experiment study clearly demonstrates that such a molecular design is not effective for solid-state applications, as only one derivative still exhibits significant emission in the crystalline form, namely the most compact one. We show that the combination of benzannulation in the presence of the strong amino donor leads to substantial changes in crystal packing and that a different network of intermolecular interactions can be found in the crystal. More specifically, going from the parent compound to its benzannulated derivatives induces a stronger π···π stacking combined with multiple CH···π interactions involving the fused benzo rings and the hydrogen atoms of the dimethylamino group, which impedes efficient emission of the crystals.

Received 15th July 2021,
Accepted 28th September 2021

DOI: 10.1039/d1tc03316f

rsc.li/materials-c

1 Introduction

Solid-state emission of organic materials remains in the limelight owing to the countless technological applications of light-emissive organic devices, *e.g.*, light-emitting diodes,[1–3] field effect transistors,[4,5] fluorescent sensors,[6,7] and laser dyes.[8,9] Development of new systems for lasing is also an important challenge in materials chemistry. A number of organic molecules are employed to that end including compounds carrying the BF_2 group.[8] The same moiety might be used to control the efficient emission of polarized light, but to fully exploit these possibilities a careful molecular design is needed[10] especially when no asymmetric atom is present in the emissive molecule but the chirality is obtained by changing the relative orientation of two moieties.[11] Likewise, efficient organics-based diodes require tweaking of the molecular structure.[12] It is now well established that molecular topology is one of the key factors in the design of efficient systems for organic electronics.[13–15] This popularity of organic fluorophores stems from their easy functionalization, making it possible to tune their photophysical properties using various synthetic and design strategies.[16] In

[a] Faculty of Chemistry, Wrocław Univ. of Science and Technology, Wyb. Wyspiańskiego 27, PL-50370 Wrocław, Poland. E-mail: robert.zalesny@pwr.edu.pl
[b] Faculty of Chemistry, Nicolaus Copernicus University, Gagarina 7, PL-87100 Toruń, Poland. E-mail: borys.osmialowski@umk.pl
[c] Laboratory of Molecular Spectroscopy, Department of Organic Chemistry, Faculty of Chemistry, University of Łódź, Tamka 12, PL-91-403, Łódź, Poland
[d] Linköping University, Department of Science and Technology, Laboratory of Organic Electronics, Norrköping, SE-60174, Sweden
[e] Department of Chemistry and Nanomaterials Science, Bohdan Khmelnytsky National University, Cherkasy, Ukraine
[f] Tomsk State University, Tomsk 634050, Russia
[g] Department of Chemistry, University of Helsinki, Helsinki FIN – 00014, Finland
[h] Department of Physics and Astronomy, Uppsala University, Box 516, SE-751 20 Uppsala, Sweden
[i] Université de Nantes, CNRS, CEISAM UMR 6230, F-44000 Nantes, France. E-mail: denis.jacquemin@univ-nantes.fr

† Electronic supplementary information (ESI) available: Data from the X-ray and spectroscopic measurements, and results from electronic-structure calculations. CCDC 2090001–2090003. For ESI and crystallographic data in CIF or other electronic format see DOI: 10.1039/d1tc03316f

particular, push–pull molecules presenting an electron-donating (D) and an electron-accepting (A) substituent separated by a π-conjugated linker are very popular.[17–19] Such molecules exhibit intramolecular charge transfer (ICT),[20,21] leading to a red-shift of the ππ* absorption band as the strength of the D and A groups and/or the delocalizable nature of the linker increases.[22,23] However, excessive ICT strength might also yield emission quenching due to the appearance of a TICT (twisted intramolecular charge transfer) or PICT (planarized intramolecular charge transfer) structure in the lowest electronic excited state, or more generally lead to a change in geometry and effective non-radiative pathways.

Another approach that makes it possible to tune the optical properties of fluorescent dyes is the fusion of benzene rings, also referred to as benzannulation.[24–27] This leads to extension of the π-conjugated skeleton, which results in beneficial red-shifts of the spectral signatures.[28,29] In addition, benzannulation comes with increased molecular rigidity which might facilitate maximizing Φ_f – a highly desired feature for many technological applications. On the other hand, large, stiff planar structures tend to stack which may lead to undesirable photophysical features in the solid state. Clar proposed an empirical rule for describing the structural features of large fused polycyclic hydrocarbons[30] which states that the system is driven toward a mesomeric structure that contains the largest number of fully delocalized π electrons. Consequently, fused rings might act as accepting groups, making benzannulation a handy approach for controlling the photophysical properties as a substitute for or in combination with more traditional accepting substituents like cyano groups.

The fluorescent dyes bearing a BF_2 group, which are our focus in the present work, are popular platforms for the above described functionalizations. Among these dyes, the BODIPY family is one of the most studied ones due to the exceptional photophysical properties: large Φ_f, high extinction coefficients, as well as narrow absorption and emission bands.[31,32] However, BODIPY dyes are known to be relatively poor for solid-state emission devices, as they suffer from aggregation caused quenching (ACQ),[33,34] notably due to reabsorption of the emitted photons by the nearby molecules, and by self-quenching due to the close contacts between the molecules (*e.g.* π-stacking) leading to the non-radiative energy dissipation. The detrimental ACQ effects can be circumvented to some extent by changing the intermolecular packing using various methods, including (i) the formation of head-to-tail aggregates *via* J-type aggregation;[35,36] (ii) the promotion of cross-stacking in the crystal structure;[37] (iii) the formation of a supramolecular co-crystal;[38,39] and (iv) the use of bulky substituents to reduce the strength of the π···π stacking interactions.[7,40] Of course, the emission properties might greatly benefit from aggregation through the opposite process, namely, aggregation induced emission (AIE).[34,41,42] The AIE phenomenon is typically caused by restriction of molecular rotational motions in solution (when the concentration of the fluorophore is close to precipitation) or in the solid state.[43,44] However, AIE has been only reported in difluoroborates, though not completely undescribed.[45–48]

As stated above the popular approach to hamper π···π stacking is to introduce bulky substituents in order to increase the intermolecular distance. Notably, it was shown that an enhancement of the Φ_f in the solid-state of perylene diimides (PDI) can be achieved by substitution with polyhedral oligomeric silsesquioxanes (POSS) at the imide position *via* either rigid or flexible linkages.[49] The studies of π-extended coumarin derivatives possessing either a seven-(DBU) or five-membered ring (DBN) attached to the core molecule also revealed differences in the photophysical properties due to different crystal packing.[50] The difference in the packing leads to fluorescence quenching in the solid state for DBN (possessing a close parallel arrangement with long-range π···π stacking) and an enhancement of Φ_f for DBU (with discrete dimeric units built by π-systems of two adjacent molecules). In another study, the influence of the π···π interactions on boron difluoride derivatives exhibiting solid state NIR-light emission was achieved by D'Aléo and co-workers.[51] The X-ray structure revealed differences in the packing modes of acetophenone and acetonaphthone-based BF_2 complexes. The latter tends to pack in a face-to-face fashion which increases the π-overlap, whereas the former yields displaced dimer units which reduces the π-contact area. This logically translated into an increase (reduction) of Φ_f in the solid state for the acetophenone (acetonaphthone)-based crystal compared to the solution. Moreover, the fine tuning of the crystal packing was used to obtain two different crystals of the same BF_2-carrying molecule characterised by completely different properties (TADF vs RTP – thermally activated delayed fluorescence vs room-temperature phosphorescence).[52]

Extensive studies of BF_2 fluorescent dyes containing NBF_2N,[53–55] NBF_2O[44,56,57] or OBF_2O[58,59] units have been reported. Some of them show bright fluorescence in the solid state.[44,51,56,60,61] We have recently shown that the optical properties of difluoroborates in solution can be tuned by combining variations of the electron-donating substituent and benzannulation of the central pyridine ring.[62–64] Such a strategy made it possible to control the strength of the donor–acceptor interactions and thus the properties of the excited states. The aim of the present work is to study the photophysical properties of crystals of the four dipolar dyes shown in Fig. 1, that all exhibit bright emission in many solvents. The use of NMe_2 group in the studied series was dictated by its high electron-donating strength and widespread presence in organic fluorescent dyes and this group hampers hydrogen bonding. More specifically we analyze the influence of benzannulation on the solid state (crystal) emission for perfectly homologous compounds, using a palette of experimental and computational methods in an

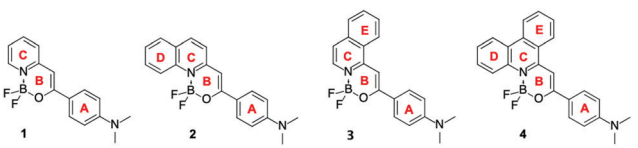

Fig. 1 Structures and ring labelling of the compounds studied herein.

effort to understand the subtle relationships between molecular structure, solution, and solid-state fluorescence.

2 Methods

2.1 Theory

2.1.1 Interaction energy partitioning scheme. Amongst the many models allowing for a decomposition of the intermolecular interaction energy,[65–72] we employ the variational–perturbational decomposition scheme (VP-EDS),[73–76] which yields components directly related to intermolecular perturbation theory.[77] In particular, the total interaction energy obtained in a supermolecular approach is partitioned into a selection of interaction energy terms analogous to the ones defined in symmetry-adapted perturbation theory (SAPT).[73–76] In VP-EDS, the total interaction energy of a dimer, calculated by a supermolecular approach in the dimer-centered-basis set (DCBS)[78] using the second-order Møller–Plesset perturbation theory (MP2) is partitioned into Hartree–Fock (HF) and the electron correlation interaction energies:

$$\Delta E_{\mathrm{int}}^{\mathrm{MP2}} = \Delta E_{\mathrm{int}}^{\mathrm{HF}} + \Delta E_{\mathrm{corr}}^{\mathrm{MP2}} \quad (1)$$

The HF term can be further partitioned into three terms representing the electrostatic interactions of unperturbed monomer charge densities, $\varepsilon_{\mathrm{el}}^{(10)}$, the associated exchange repulsion, $\Delta E_{\mathrm{ex}}^{\mathrm{HL}}$, and the charge delocalization, $\Delta E_{\mathrm{del}}^{\mathrm{HF}}$, which encompasses the induction and the associated exchange effects due to the Pauli exclusion principle:

$$\Delta E_{\mathrm{int}}^{\mathrm{HF}} = \varepsilon_{\mathrm{el}}^{(10)} + \Delta E_{\mathrm{ex}}^{\mathrm{HL}} + \Delta E_{\mathrm{del}}^{\mathrm{HF}} \quad (2)$$

Note that the indices in parentheses denote perturbation orders in the intermolecular interaction operator and intramonomer correlation operator, respectively. In this notation, the second-order electron correlation term, $\Delta E_{\mathrm{corr}}^{\mathrm{MP2}}$,

$$\Delta E_{\mathrm{corr}}^{\mathrm{MP2}} = \varepsilon_{\mathrm{el,r}}^{(12)} + \varepsilon_{\mathrm{disp}}^{(20)} + \Delta E_{\mathrm{ex}}^{(2)} \quad (3)$$

includes the second order dispersion interaction, $\varepsilon_{\mathrm{disp}}^{(20)}$, the electron correlation correction to the first order electrostatic interaction, $\varepsilon_{\mathrm{el,r}}^{(12)}$, and the remaining electron correlation effects, $\Delta E_{\mathrm{ex}}^{(2)}$. The latter term accounts mainly for the uncorrelated exchange–dispersion and electron correlation corrections to the Hartree–Fock exchange repulsion.[75,77] Both $\varepsilon_{\mathrm{el}}^{(10)}$ and $\varepsilon_{\mathrm{disp}}^{(20)}$ are obtained in the standard polarization perturbation theory, whereas $\varepsilon_{\mathrm{el,r}}^{(12)}$ is calculated using the formula proposed by Moszyński *et al.*[79]

2.1.2 Computational details. The intermolecular interaction energies and their components were calculated using the Kohn–Sham formulation of Density Functional Theory (DFT), MP2, and its spin-component-scaled variant (SCS-MP2)[80] for the dimer complexes composed of **1–4**, using experimentally determined crystallographic geometries. All calculation were performed using a supermolecular approach with counterpoise correction.[81] At the DFT level, a range-separated exchange–correlation functional including an empirical dispersion term, namely ωB97X-D[82], is used. These DFT calculations were performed using the Gaussian 16 program[83] with Dunning's correlation consistent basis sets (aug-cc-pVDZ and aug-cc-pVTZ).[84–86] While the triple-ζ basis set is obviously more accurate and yields smaller basis set superposition errors (BSSE) than its double-ζ counterpart, the number of basis functions exceeds 3000 with the larger basis for the dimers. The calculations presented in this work were therefore performed using the aug-cc-pVDZ basis set, the difference in total interaction energies obtained with the two basis sets being in the 0.3–0.8 kcal mol^{-1} range (Table S9, ESI†). Unfortunately, even the aug-cc-pVDZ (1700 basis functions on average) is computationally untractable at the MP2 level, and we resort to the density fitting approach (also known as resolution-of-the-identity or RI) at both the HF and MP2 levels.[87–91] The second-order electron correlation term, $\Delta E_{\mathrm{corr}}^{\mathrm{MP2}}$ was determined as

$$\Delta E_{\mathrm{corr}}^{\mathrm{MP2}} = \Delta E_{\mathrm{int}}^{\mathrm{MP2}} - \Delta E_{\mathrm{int}}^{\mathrm{HF}} \quad (4)$$

The HF term was obtained and further partitioned as described above by applying the VP-EDS scheme on the HF/aug-cc-pVDZ data using a modified version of the GAMESS US code.[92,93] The $\Delta E_{\mathrm{int}}^{\mathrm{MP2}}$ term is calculated using density fitting with the same basis set using MOLPRO.[94]

For the simulations of the optical properties, the molecular structures of the ground singlet state were optimized at the DFT level using the B3LYP[95] functional and the 6-31G(d,p)[96] basis set. Excitation energies were calculated in the gas phase using both the extended multiconfiguration quasidegenerate perturbation theory at the second order level (XMC-QDPT2)[97] and time-dependent density functional theory (TD-DFT).[98] The XMC-QDPT2 calculations were performed using the Firefly software[99] with active spaces consisting of 10 electrons in 10 molecular orbitals (see Table S11, ESI†). The non-adiabatic coupling matrix elements (NACME) were calculated using Turbomole.[100] The spin–orbit coupling matrix elements (SOCME) between the first singlet excited state and the lowest triplet state were calculated using the PySOC software[101] based on the Breit–Pauli (BP) spin–orbit Hamiltonian with an effective charge approximation. The internal conversion (IC) and intersystem crossing (ISC) rate constants were calculated within the Herzberg–Teller approximation[102,103] taking into account the anharmonicity effects.[104] The IC rate constants (k_{ic}) were obtained using the algorithm published elsewhere,[105] which assumes that the X–H vibrations mainly contribute to the IC process.

2.2 Experiment

The description of synthesis and full characterization of compounds in solution by ^{1}H, ^{11}B, ^{13}C, ^{15}N and ^{19}F NMR spectroscopy and elemental analysis can be found in ref. 19 and 106 (**1**), ref. 107 (**2**), ref. 63 (**3**) and ref. 64 (**4**). The X-ray data were collected at 293(2) K using an Oxford Sapphire CCD diffractometer using MoKα radiation (λ = 0.71073 Å). The structures were solved by direct methods and refined using the full-matrix least-squares method on F^2 with the use of SHELX2017 program package.[108] The analytical absorption corrections were applied by CrysAlis 171.38.43 package of programs Rigaku OD.[109]

The C-bonded hydrogen atom positions were calculated from geometry. All hydrogen atoms were constrained during refinement. A summary of the crystal data and refinement details for compounds **2–4** is given in Table S6 (ESI†). CCDC 2090001 for **2** and 2090002 for **3**, and 2090003 for **4**. Emission spectra of solid-state samples of **1–4** were recorded on a Fluoromax-4 (Horiba) spectrofluorometer equipped with a long pass filter and the fluorescence quantum yields were measured using the same apparatus equipped with an integrating sphere Quanta.

3 Results

3.1 Photophysical properties

Previously we showed that the benzannulation position has a significant impact on the fluorescence features in solution.[62–64,110] The Φ_f of **1–4** measured in the various solvents are listed in Table 1 (see also Table S1, ESI†). All compounds exhibit bright emission in solution, the Φ_f's magnitude being dependent on the nature of the solvent. The largest Φ_f is observed in diethyl ether (Et_2O) for **1**, and in methylcyclohexane (MCH) for **2–4**. As shown in Table S1 (ESI†), changing the solvent polarity influences both the radiative (k_r) and non-radiative (k_{nr}) constants. Illustratively, passing from MCH to dimethylformamide (DMF) k_r is decreasing and k_{nr} is increasing.

In order to gain insight into the fluorescence properties of **1–4**, and more specifically on the rates of the radiative and non-radiative decay pathways, we first performed gas-phase calculations carried out at the TD-DFT/B3LYP/6-31G(d,p) and XMC-QDPT2/6-31G(d,p) levels of theory. The results are presented in Tables S2–S5 in the ESI.† Tables S4 and S5 (ESI†) show that the TD-DFT predicts twice larger S_1–T_1 energy gaps and much smaller SOCME values than XMC-QDPT2. As a consequence, TD-DFT foresees internal conversion as the main deactivation pathway, while XMC-QDPT2 predicts intersystem crossing to be a competitive deactivation channel (compare Tables S3 and S5, ESI†). Despite this difference in prediction of non-radiative deactivation rate constants, both levels of theory show that the radiative rate constant dominates over the IC and ISC deactivation channels for all molecules. The prevalence of the k_r over k_{nr} agrees with the experimental data measured in the least polar solvents such as MCH and Et_2O (Table S1, ESI†). It is mainly due to the exponential growth of the internal conversion efficiency with the decrease of the S_1–S_0 energy gap.[111,112] Indeed, the polar solvents affect the bathochromic shift of the emission wavelengths for all molecules (Table S1, ESI†)

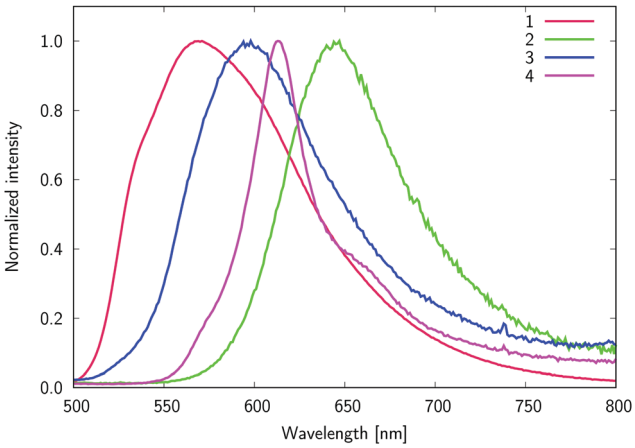

Fig. 2 Solid-state fluorescence of the investigated compounds.

which results in a monotonous decrease of the fluorescence quantum yield. Thus, although the obtained theoretical data indicate non-zero values of SOCME and NACME for the coupling between the S_1–T_1 and S_1–S_0 states, respectively, the quite large values of the S_1–S_0 vertical transition energies and oscillator strengths for **1–4** hint that fluorescence dominates over the non-radiative processes for the single molecules.

In order to study the photophysical properties in the solid state, crystals of **1–4** were obtained by slow evaporation of the chloroform solution. The solid state fluorescence spectra are displayed in Fig. 2 and the measured Φ_f values are listed in Table 1. The emission bands are red-shifted in the crystal as compared to in the solution, with peaks at **1** (563 nm) < **3** (600 nm) < **4** (611 nm) < **2** (645 nm) in the solid state. More interestingly, while these measurements confirm that benzannulation significantly affects the emission properties, rather different patterns were obtained in solution and in the crystal, with very strong quenching of the fluorescence for **2–4** and with bright emission for **1** only in the latter phase. The fluorescence lifetimes of compounds **1** and **4** in the solid state are 9.64 μs and 8.93 μs, respectively. For compounds **2** and **3**, exhibiting very low fluorescence quantum yields, the results are not reliable due to the spectrometer limitations. The lifetimes measured in the solid state are three orders of magnitude higher than that determined in chloroform solution.[19,62–64,106]

3.2 Molecular packing

To understand the fundamental origins of these striking differences between the emission measured for solutions and

Table 1 Fluorescence quantum yields of **1–4** measured in different solvents[a] and in the solid-state

Comp.	MCH[b]	Et_2O[c]	THF[d]	EA[e]	AcMe[f]	MeOH[g]	MeCN[h]	DMF[i]	SS[j]
1	0.519	0.868	0.684	0.699	0.569	0.454	0.517	0.382	0.314
2	0.862	0.747	0.517	0.614	0.374	0.308	0.296	0.187	<0.01
3	0.979	0.848	0.658	0.663	0.587	0.499	0.638	0.561	0.020
4	1.000	0.999	0.585	0.655	0.441	0.471	0.447	0.323	0.063

[a] Solvents in the table are ordered according to increasing magnitude of their dipole moment. [b] Methylcyclohexane. [c] Diethyl ether. [d] Tetrahydrofuran. [e] Ethyl acetate. [f] Acetone. [g] Methanol. [h] Acetonitrile. [i] Dimethylformamide. [j] Solid state.

crystals, first we analyze the packing of each dye and the intermolecular interactions. To this end, we analyze published X-ray measurements for **1**,[106] and use crystal structures determined in the present work for the other three dyes, and additionally further considered a parent, unsubstituted compound of **4** (denoted as **4(H)** below), which was studied by Wu and co-workers[56] and is available in the CCDC database. The crystal structure information and the detailed description of the molecular packing of **2–4** are given in the ESI.† The crystals of **1**, **3**, and **4** correspond to orthorhombic and **2** to triclinic crystal systems with the space groups $Pca2_1$, *Pbca*, *Pbca*, and $P\bar{1}$, respectively. The molecular packing as well as the main interactions and dimers of **1–4** selected for further studies are depicted in Fig. 3. The asymmetric unit of the structure for compound **1** consists of **2** molecules – **a** (red) and **b** (blue) in Fig. 3a. The π···π interactions are found between the pyridine rings C (labeling of the rings can be found in Fig. 1) of molecule **a** and molecule **b** in the $\mathbf{1ba}_{\pi\pi}$ dimer. A series of C–H···π interactions are also present in that structure between the pyridine C and aniline A rings of both molecules, leading to that the $\mathbf{1ab}_{\mathrm{Tp}}$–**1** and $\mathbf{1ab}_{\mathrm{Tp}}$–**2** dimers show edge-to-face T-shape and weak (due to the angle between rings) π···π stacking, see Fig. 3a. Only a single molecule, **a**, of **2** is found in the asymmetric part of the crystal structure. The X-ray crystallographic analysis reveals several π···π interactions between the C and A rings. In addition, the methyl group of the aniline moiety (ring A) is involved in C–H···π interactions with the ring D.

Both interaction types are found in the two types of head-to-tail dimers, $\mathbf{2aa}_{\pi\pi}$–**1** and $\mathbf{2aa}_{\pi\pi}$–**2**, which have a parallel displaced stacked configuration (Fig. 3b). For the isoquinoline derivative **3**, the asymmetric unit contains **3** molecules – **a** (red), **b** (blue), and **c** (green), see Fig. 3c. π···π-type stacks are found only between equivalent molecules leading to the $3aa_{\pi\pi}$, $3bb_{\pi\pi}$, $3cc_{\pi\pi}$ dimers, see the left-hand side of Fig. 3c. The dominating π···π interactions take place between the B and C (C and E) rings for molecules **c** (**a** and **b**). C–H···π interactions are found between the methyl of the NMe_2 groups and the A rings. For further analysis, we also consider the dimers with edge-to-face T-shape π···π stacking ($\mathbf{3bb}_{\mathrm{Tp}}$ and $\mathbf{3ca}_{\mathrm{Tp}}$) and C–H···π interactions ($\mathbf{3ba}_{\mathrm{CHp}}$ and $\mathbf{3cc}_{\mathrm{CHp}}$). For the phenanthridine derivative, **4**, only one molecule type (a) is present. Two types of dimers can be evidenced: $\mathbf{4aa}_{\pi\pi}$ formed by π···π interactions between the C and E rings, and $\mathbf{4aa}_{\mathrm{CHp}}$ characterized by C–H···π interactions between the methyl group of the aniline moiety and ring A (Fig. 3d). Finally, as can be seen in Fig. 3e, the molecular packing for **4(H)** suggests only π···π interactions between the phenanthridine derivatives **4(H)**, leading to the $\mathbf{4(H)}_{\pi\pi}$ dimer.

3.3 Intermolecular interaction energy decomposition

The above analysis of packing modes reveals quite different structural motifs which require further characterization. To this end, we performed quantum-chemical calculations (see Methods section) to shed light onto the strength of these interactions and unravel their physical origin. The calculated intermolecular interaction energies together with their decomposition according to the VP-EDS scheme for representative dimers (see Fig. 3 and Table S10 in the ESI†) are given in Table 2 and in Fig. 4. In that Table, we provide the interaction energies obtained with the ωB97X-D functional, MP2, and SCS-MP2. The dimer complexes with π···π stacking, especially in compounds **3**, **4**, and **4(H)**, have total interaction energies $\Delta E_{\mathrm{int}}^{\mathrm{MP2}}$ larger (by up to 3.1 kcal mol^{-1}) than the corresponding $\Delta E_{\mathrm{int}}^{\mathrm{wB97X\text{-}D}}$ energies. It is indeed the usual trend,[113] that MP2 overestimates the π···π stacking intermolecular interaction energies. This overestimation, due to the uncoupled dispersion energy term, tends to be systematic and does not hamper the analysis of the intermolecular interaction energies of the different stacking motifs. As discussed above, there are three main interaction types in the crystals: parallel displaced π···π stacking, edge-to-face T-shape together with weak π···π stacking (T-shape + π···π), and C–H···π intermolecular interactions. The strength of the interaction energies increases in the following order C–H···π < T-shape + π···π < parallel displaced π···π complexes (Fig. 4). Nevertheless, for dimer $\mathbf{4aa}_{\mathrm{CHp}}$ the total interaction energy is comparable to those determined for T-shape + π···π stacked dimers. We also note that the strength of the π···π interactions is very similar for **4** and **4(H)** which, as discussed in the next Section, have very different emission properties in the solid state. The calculations highlight the key role of the electrostatic and electron correlation terms (which include the uncoupled dispersion term) for the selected dimers; these two components determine the intermolecular interaction energies for the π-stacked complexes of **2–4** and **4(H)**. It can be seen that the exchange repulsion term, which is a destabilizing contribution, plays a significant role in the π-stacked dimers but has a trifling impact on the complexes based on C–H···π interactions.

4 Discussion

In the Introduction, we argued that the π···π interactions play an important role not only in determining the crystal packing but also in tuning the solid state emission. However, the C–H···π interaction or the stronger intermolecular hydrogen bonds may also have a considerable effect, as clearly shown by the data presented above. In what follows we relate literature conclusions to our findings of the Φ_{f} of the crystals.

4.1 Literature survey

The studies of the correlation between molecular packing and photophysical properties for *N*-methylpyrazoline derivatives demonstrated the impact of the intermolecular interactions present in the crystal lattice.[114] The comparison of relative contributions of different close contacts with their fluorescence characteristics revealed that higher relative contributions of H···O and H···N contacts yield enhanced non-radiative decay, and consequently fluorescence quenching. Similarly, the links between molecular packing and substitution effects were recently established for chalcone crystals with a focus on the balance between red emissive and photodimerization-triggered hopping behaviour.[115] By changing the nature of the amino

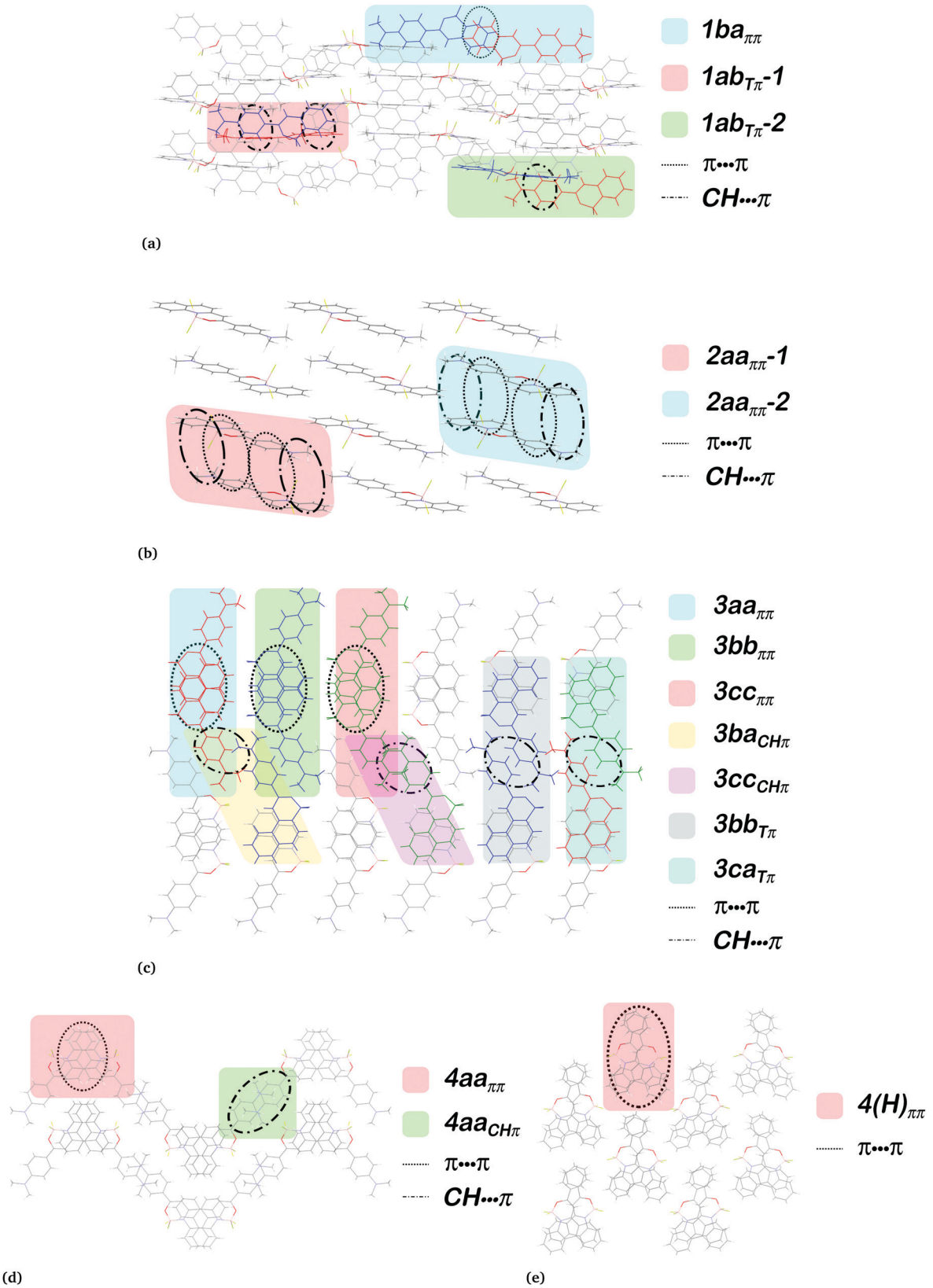

Fig. 3 Molecular packing of **1** (a), **2** (b), **3** (c), **4** (d), and **4(H)** (e) with the indication of the main types of intermolecular interactions and key dimers that are studied herein.

Table 2 Results of intermolecular interaction energy calculations[a]

Dimer	Total interaction energies				Decomposition of MP2 energies			
	$\Delta E_{int}^{\omega B97X\text{-}D}$	ΔE_{int}^{MP2}	$\Delta E_{int}^{SCS\text{-}MP2}$	ΔE_{int}^{HF}	$e_{el}^{(10)}$	ΔE_{ex}^{HL}	ΔE_{del}^{HF}	ΔE_{corr}^{MP2}
1								
1ba$_{\pi\pi}$	−11.07	−11.20	−8.99	−1.85	−7.91	7.58	−1.52	−9.35
1ab$_{T\pi}$–**1**	−11.66	−11.20	−7.91	2.86	−2.92	7.18	−1.40	−14.06
1ab$_{T\pi}$–**2**	−13.70	−12.90	−10.45	−2.58	−6.57	5.7	−1.71	−10.32
2								
2aa$_{\pi\pi}$-	−25.00	−25.27	−18.47	4.61	−8.98	16.68	−3.09	−29.88
1								
2aa$_{\pi\pi}$–**2**	−26.26	−28.23	−20.96	3.81	−11.34	18.52	−3.37	−32.04
3								
3aa$_{\pi\pi}$	−18.21	−20.58	−14.81	5.29	−10.45	18.68	−2.94	−25.87
3bb$_{\pi\pi}$	−17.30	−19.53	−14.14	4.58	−9.47	16.53	−2.48	−24.11
3cc$_{\pi\pi}$	−17.39	−19.67	−14.43	3.77	−9.08	15.14	−2.29	−23.44
3bb$_{T\pi}$	−13.34	−12.57	−10.61	−4.26	−6.04	3.15	−1.37	−8.31
3ba$_{CH\pi}$	−5.52	−4.76	−3.44	1.09	−1.77	3.34	−0.48	−5.85
3cc$_{CH\pi}$	−7.36	−6.65	−4.95	0.92	−2.66	4.27	−0.69	−7.57
3ca$_{T\pi}$	−13.88	−13.35	−11.35	−4.80	−6.58	3.32	−1.54	−8.55
4								
4aa$_{\pi\pi}$	−22.87	−25.96	−19.04	4.76	−10.68	18.56	−3.12	−30.72
4aa$_{CH\pi}$	−12.10	−11.32	−8.98	−0.94	−4.94	5.04	−1.04	−10.38
4(H)								
4(H)$_{\pi\pi}$	−25.74	−28.34	−20.55	6.26	−10.03	19.45	−3.16	−34.60

[a] All values are given in kcal mol^{-1}. All calculations were performed using the aug-cc-pVDZ basis set. The description of intermolecular interaction energies components is given in the Methods section.

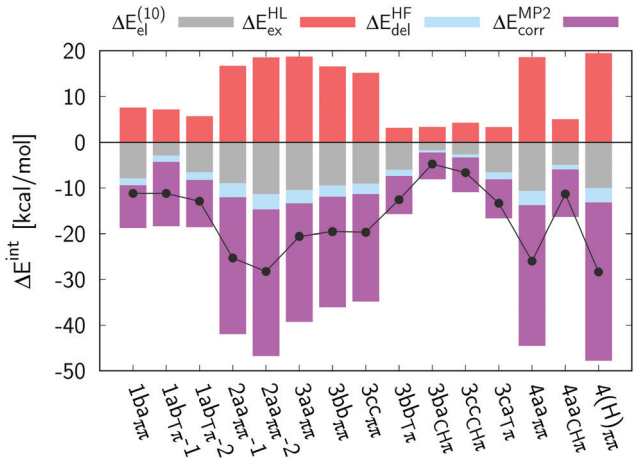

Fig. 4 Decomposition of RI-MP2/aug-cc-pVDZ intermolecular interaction energy into electrostatic, exchange, delocalization, and electron correlation contributions for studied dimers of **1–4** and compound **4(H)**. The solid line corresponds to the sum of all components.

group two different crystal arrangements with anti-parallel packing have been obtained: (i) NMe_2-bearing chalcone derivatives with face-to-face alignment of the D and A groups, as well as multiple C–H···π interactions; (ii) NPh_2-substituted chalcone compounds without D–A stacking. Whilst the two compounds develop similar photophysical properties in solution, only the latter molecule is bright in the crystal. Iwasaki and co-workers reported that different alkyl chains can affect the solid-state photophysical properties of 1,3,6,8-tetraalkylpyrenes.[116] Their investigation indicates that alkyl groups modify the crystal packing, which significantly affects both the emission colour and the quantum yield.

As illustrated by the above examples, a dense network of weak intermolecular interactions can quench the fluorescence; however, there are many examples in which it is the interplay between strong π···π and other types of weaker interactions that dictates the final response. Illustratively, the influence of π···π interactions on the solid-state emission properties of triphenylamino benzothiazole-based fluorogens undergoing (or not) excited-state intramolecular proton transfer (ESIPT) have been studied by Padalkar *et al.*[117] The face-to-face arrangements of dimers in the crystal structure are responsible for the presence of strong π···π stacking which, along with other intermolecular interactions (C–H···π, C–H···O, C–H···N), hinder both the ESIPT and the fluorescence processes. 7-Amino and 4-methyljulolydyl coumarin crystals have a network of hydrogen bonds and/or π···π stacking interactions, leading to very weak solid-state fluorescence.[118] In contrast, 7-diethylamino coumarin dyes that form isolated monomer- and dimer-type stacking show intense fluorescence. Eventually, an investigation of the molecular packing of isomeric benzofuranonaphthoquinol-type fluorophores made it possible to rationalize the fluorescence quenching of phenyl substituted compounds.[119] Indeed, the crystal data confirmed the presence of hydrogen bonds and strong π···π interactions explaining the low emission of these molecules in the solid state. Interestingly, enhanced Φ_f could be achieved by changing the hydroxy (–OH) to the butoxy (–OBu) group which leads to packing with reduced interaction strengths.

The above-mentioned studies show that packing and photophysical properties of crystals are significantly influenced by various types of intermolecular interactions originating from the molecular structure. The increase of Φ_f in the solid state can be achieved (i) by suppressing hydrogen bonding (H···O and H···N contacts) and π···π interactions using the –OBu, methoxy (–OMe), or acetyl (–COOMe) group as a substituent rather than the –OH group; (ii) by reducing the network of hydrogen bonds and C–H···π interactions as well as π···π stacking using the NPh_2 or diethylamino (NEt_2) group instead of the NMe_2 or amino (NH_2) group. In short, the weaker the intermolecular interactions the higher the fluorescence in the solid state.

4.2 Analysis of compounds 1–4

The data obtained in the present study partially parallel the findings summarized above. We recall that the analysis of the molecular packing revealed the following similarities within the crystal structures presented in this work: the packing of **1–4** is characterized by π···π and CH···π interactions, while only π···π stacking is found in the **4(H)** crystal. The intermolecular interaction energy calculations of the corresponding dimers (Table 2) indicated that the **1ba**$_{\pi\pi}$ dimer exhibits much weaker π···π interactions than any of the dimers of **2**, **3**, **4**, and **4(H)** in π···π stacked alignment. On the other hand, the T-shape π···π

stacked complexes of **1**, **3**, and $\mathbf{4aa}_{CHp}$ exhibit similar intermolecular interaction energies to that found in the $\mathbf{1ba}_{\pi\pi}$ dimer. This energetic analysis can be linked with the finding that the crystal of **1**, formed by C–H$\cdots\pi$ and weak $\pi\cdots\pi$ interactions, possesses moderate Φ_f. The molecular packing of **2**, **3** and **4**, exhibiting strong $\pi\cdots\pi$ stacking and several CH$\cdots\pi$ interactions, leads to quenching of the fluorescence in the solid state. However, the strong $\pi\cdots\pi$ interactions present in the crystal of **4(H)** do not have a detrimental effect on fluorescence quantum yield and green emission is observed for this crystal.[56] In the case of **2**, **3**, and **4** one finds multiple CH$\cdots\pi$ interactions involving fused benzene rings and the hydrogen atoms of the dimethylamino group. It follows from our comparative analysis of (**1** *vs.* **2–4** and **4** *vs.* **4(H)**) that these additional interaction modes are detrimental as far as the emission of the crystals is concerned. Based on our findings we can propose that the strategy to tune photophysical properties of topologically similar dyes that aims at retaining high Φ_f values in the solid-state should consider (i) changing the dimethylamino group to diethylamino, which can reduce the dense network of CH$\cdots\pi$ interactions; and (ii) using bulky piperidine or dibutylamino moieties instead of the NMe_2 group that can increase the spacing between aromatic rings, therefore decrease the energy of $\pi\cdots\pi$ interactions.

5 Conclusions

In this work we have studied the emission properties of a series of four fluoroborate organic dyes. These dipolar compounds contain an electron-donating $N(CH_3)_2$ group and various NBF_2O-containing heterocyclic moieties acting as electron-accepting units. The members of the series differ in the number and positions of the fused benzene rings in the heterocyclic part. These compounds exhibit strong emission in solution, with fluorescence quantum yields exceeding 0.8 for each member of the series in at least one of the solvents used, regardless of the benzannulation type. The theoretical calculations performed on the isolated structures highlight the dependence between the S_1 state energy and the Φ_f. The fluorescence efficiency is quenched with decrease of the S_1-S_0 gap, which logically increases the rate constants for internal conversion. This analysis is confirmed by the experimental data: a redshift of the fluorescence maximum caused by an increase of the solvent polarity induces a drastic decrease of the Φ_f for all fluorophores. The increase of the dipolar character, achieved by substitution by the $N(CH_3)_2$ group and benzannulation, enhances the photoinduced charge transfer nature and is an effective strategy to tune the photophysical properties of these dyes in solution, *i.e.*, it allows a redshift of the absorption spectra without deterioration of the emission properties. Moreover, the present work clearly demonstrates that this is not an effective strategy in the solid state, or more precisely, that more refined strategies need to be used for maximizing the emission brightness of the crystals. Indeed, only one crystal of the studied series exhibits a significant emission. The various benzannulation schemes yield substantial changes in the crystal packing and new interaction types between the molecules in the unit cells. More specifically, on passing from the parent compound to its benzannulated derivatives one finds stronger $\pi\cdots\pi$ stacking supplemented by multiple additional CH$\cdots\pi$ interactions involving the fused benzene rings and the hydrogen atoms of the dimethylamino group. It follows from our comparative analysis that these new interactions are detrimental as far as emission from the crystals is concerned. The strategy for tuning the photophysical properties of similar dyes, aiming at retaining high Φ_f values in the solid state, should avoid combinations of moieties with multiple fused rings as well as groups facilitating CH$\cdots\pi$ interactions.

Author contributions

Conceptualization (B. O., R. Z.). Investigation (I. K., A. K., A. W., D. P., G. B., R. V., R. N., B. O., R. Z.). Methodology (I. K., D. J., B. O., R. Z.). Project administration (B. O., R. Z.). Software (H. A., G. B., R. V.). Validation (I. K., G. B., R. V., R. N., R. Z.). Visualization (I. K., A. K., A. W., G. B., R. V., R. Z.). Writing-original draft (I. K., A. W., D. J., B. O., R. Z.). Writing-review and editing (all authors).

Conflicts of interest

There are no conflicts to declare.

Acknowledgements

B. O. and R. Z. acknowledge financial support from the Polish National Science Centre (Grant No. 2017/26/M/ST5/00327). A. K. and A. W. acknowledge the partial support of the Center of Excellence ''Towards Personalized Medicine'' operating under Excellence Initiative-Research University (NCU). G. B. thanks the Swedish Research Council (starting grant No. 2020-04600) and the Ministry of Education and Science of Ukraine (project no. 0121U107533) for support. This work has also been supported by the Academy of Finland through projects 1325369, 1315600 (R. V.). R. V. thanks the Decree of the Government of the Russian Federation N. 220 of 09 April 2010 (Agreement No. 075-15-2021-615 of 4 June 2021). The computations were enabled by resources provided by the Swedish National Infrastructure for Computing (SNIC) at the High Performance Computing Center North (HPC2N) partially funded by the Swedish Research Council through grant agreement no. 2020/3-29. Calculations were also performed at the Wroclaw Center for Networking and Supercomputing. The Wroclaw and Nantes team are indebted to the CNRS for supporting their collaboration in the framework of the ABSOLUTA-IEA grant. D. J. thanks the CCIPL computational center installed in Nantes for the generous allocation of computational time. The authors thank Lizaveta Petrusevich for the preparation of the graphical TOC entry.

References

1 J. Liu, H. Zhang, H. Dong, L. Meng, L. Jiang, L. Jiang, Y. Wang, J. Yu, Y. Sun, W. Hu and A. J. Heeger, *Nat. Commun.*, 2015, **6**, 10032.
2 X. Yang, G. Zhou and W.-Y. Wong, *Chem. Soc. Rev.*, 2015, **44**, 8484–8575.
3 A. Zampetti, A. Minotto, B. M. Squeo, V. G. Gregoriou, S. Allard, U. Scherf, C. L. Chochos and F. Cacialli, *Sci. Rep.*, 2017, **7**, 1611.
4 F. Cicoira and C. Santato, *Adv. Funct. Mater.*, 2007, **17**, 3421–3434.
5 C. Wang, X. Ren, C. Xu, B. Fu, R. Wang, X. Zhang, R. Li, H. Li, H. Dong, Y. Zhen, S. Lei, L. Jiang and W. Hu, *Adv. Mater.*, 2018, **30**, 1706260.
6 L. Basabe-Desmonts, D. N. Reinhoudt and M. Crego-Calama, *Chem. Soc. Rev.*, 2007, **36**, 993–1017.
7 G.-L. Fu, H. Pan, Y.-H. Zhao and C.-H. Zhao, *Org. Biomol. Chem.*, 2011, **9**, 8141–8146.
8 Y. Jiang, Y.-Y. Liu, X. Liu, H. Lin, K. Gao, W.-Y. Lai and W. Huang, *Chem. Soc. Rev.*, 2020, **49**, 5885–5944.
9 R. Aoki, R. Komatsu, K. Goushi, M. Mamada, S. Y. Ko, J. W. Wu, V. Placide, A. D'Aléo and C. Adachi, *Adv. Opt. Mater.*, 2021, **9**, 2001947.
10 J. Li, X. Peng, C. Huang, Q. Qi, W.-Y. Lai and W. Huang, *Polym. Chem.*, 2018, **9**, 5278–5285.
11 J. Li, C. Hou, C. Huang, S. Xu, X. Peng, Q. Qi, W.-Y. Lai and W. Huang, *Research*, 2020, 3839160.
12 Y. Xu, P. Xu, D. Hu and Y. Ma, *Chem. Soc. Rev.*, 2021, **50**, 1030–1069.
13 C.-F. Liu, X. Liu, W.-Y. Lai and W. Huang, *Chem. Rec.*, 2019, **19**, 1571–1595.
14 X. Liu, M. Sang, H. Lin, C. Liu, J. Zhang, J. Yi, K. Gao, W.-Y. Lai and W. Huang, *Chem. – Eur. J.*, 2020, **26**, 3103–3112.
15 T. P. I. Saragi, T. Spehr, A. Siebert, T. Fuhrmann-Lieker and J. Salbeck, *Chem. Rev.*, 2007, **107**, 1011–1065.
16 S. P. Anthony, *ChemPlusChem*, 2012, **77**, 518–531.
17 S. Xu, R. E. Evans, T. Liu, G. Zhang, J. N. Demas, C. O. Trindle and C. L. Fraser, *Inorg. Chem.*, 2013, **52**, 3597–3610.
18 A. M. Grabarz, A. D. Laurent, B. Jedrzejewska, A. Zakrzewska, D. Jacquemin and B. Osmiałowski, *J. Org. Chem.*, 2016, **81**, 2280–2292.
19 B. Jedrzejewska, A. Skotnicka, A. D. Laurent, M. Pietrzak, D. Jacquemin and B. Osmiałowski, *J. Org. Chem.*, 2018, **83**, 7779–7788.
20 Y.-Y. Wu, Y. Chen, G.-Z. Gou, W.-H. Mu, X.-J. Lv, M.-L. Du and W.-F. Fu, *Org. Lett.*, 2012, **14**, 5226–5229.
21 J. Chen, W. Liu, J. Ma, H. Xu, J. Wu, X. Tang, Z. Fan and P. Wang, *J. Org. Chem.*, 2012, **77**, 3475–3482.
22 E. Kim, A. Felouat, E. Zaborova, J.-C. Ribierre, J. W. Wu, S. Senatore, C. Matthews, P.-F. Lenne, C. Baffert, A. Karapetyan, M. Giorgi, D. Jacquemin, M. Ponce-Vargas, B. L. Guennic, F. Fages and A. D'Aléo, *Org. Biomol. Chem.*, 2016, **14**, 1311–1324.
23 S. Redon, G. Eucat, M. Ipuy, E. Jeanneau, I. Gautier-Luneau, A. Ibanez, C. Andraud and Y. Bretonnière, *Dyes Pigm.*, 2018, **156**, 116–132.
24 Y. Avlasevich, C. Li and K. Müllen, *J. Mater. Chem.*, 2010, **20**, 3814–3826.
25 K. Hanson, L. Roskop, P. I. Djurovich, F. Zahariev, M. S. Gordon and M. E. Thompson, *J. Am. Chem. Soc.*, 2010, **132**, 16247–16255.
26 K. Kurotobi, K. S. Kim, S. B. Noh, D. Kim and A. Osuka, *Angew. Chem., Int. Ed.*, 2006, **45**, 3944–3947.
27 M. J. Kuisma, A. M. Lundin, K. Moth-Poulsen, P. Hyldgaard and P. Erhart, *J. Phys. Chem. C*, 2016, **120**, 3635–3645.
28 R. Gresser, M. Hummert, H. Hartmann, K. Leo and M. Riede, *Chem. – Eur. J.*, 2011, **17**, 2939–2947.
29 S. Yamazawa, M. Nakashima, Y. Suda, R. Nishiyabu and Y. Kubo, *J. Org. Chem.*, 2016, **81**, 1310–1315.
30 E. Clar, *Aromatic Sextet*, Willey, London, 1972.
31 R. Ziessel, G. Ulrich and A. Harriman, *New J. Chem.*, 2007, **31**, 496–501.
32 J. Bañuelos, *Chem. Rec.*, 2016, **16**, 335–348.
33 J. B. Birks, *Photophysics of Aromatic Molecules*, Wiley, London, 1970.
34 J. Mei, N. L. C. Leung, R. T. K. Kwok, J. W. Y. Lam and B. Z. Tang, *Chem. Rev.*, 2015, **115**, 11718–11940.
35 S. Kim, J. Bouffard and Y. Kim, *Chem. – Eur. J.*, 2015, **21**, 17459–17465.
36 D. Kim, U. Lee, J. Bouffard and Y. Kim, *Adv. Opt. Mater.*, 2020, **8**, 1902161.
37 Z. Xie, B. Yang, F. Li, G. Cheng, L. Liu, G. Yang, H. Xu, L. Ye, M. Hanif, S. Liu, D. Ma and Y. Ma, *J. Am. Chem. Soc.*, 2005, **127**, 14152–14153.
38 D. Yan, A. Delori, G. O. Lloyd, T. Friščić, G. M. Day, W. Jones, J. Lu, M. Wei, D. G. Evans and X. Duan, *Angew. Chem., Int. Ed.*, 2011, **50**, 12483–12486.
39 L. Sun, W. Zhu, W. Wang, F. Yang, C. Zhang, S. Wang, X. Zhang, R. Li, H. Dong and W. Hu, *Angew. Chem., Int. Ed.*, 2017, **56**, 7831–7835.
40 T. Ozdemir, S. Atilgan, I. Kutuk, L. T. Yildirim, A. Tulek, M. Bayindir and E. U. Akkaya, *Org. Lett.*, 2009, **11**, 2105–2107.
41 Y. Hong, J. W. Y. Lam and B. Z. Tang, *Chem. Soc. Rev.*, 2011, **40**, 5361–5388.
42 Y. Yang, X. Su, C. N. Carroll and I. Aprahamian, *Chem. Sci.*, 2012, **3**, 610–613.
43 Y. Hong, J. W. Y. Lam and B. Z. Tang, *Chem. Commun.*, 2009, 4332–4353.
44 Y. Kubota, K. Kasatani, H. Takai, K. Funabiki and M. Matsui, *Dalton Trans.*, 2015, **44**, 3326–3341.
45 H. Gao, D. Xu, X. Liu, A. Han, L. Zhou, C. Zhang, Y. Yang and W. Li, *RSC Adv.*, 2017, **7**, 1348–1356.
46 S. Gong, Q. Liu, X. Wang, B. Xia, Z. Liu and W. He, *Dalton Trans.*, 2015, **44**, 14063–14070.
47 F. Qi, J. Lin, X. Wang, P. Cui, H. Yan, S. Gong, C. Ma, Z. Liu and W. Huang, *Dalton Trans.*, 2016, **45**, 7278–7284.
48 Y. Wu, Z. Li, Q. Liu, X. Wang, H. Yan, S. Gong, Z. Liu and W. He, *Org. Biomol. Chem.*, 2015, **13**, 5775–5782.
49 Y. Shao, G.-Z. Yin, X. Ren, X. Zhang, J. Wang, K. Guo, X. Li, C. Wesdemiotis, W.-B. Zhang, S. Yang, M. Zhu and B. Sun, *RSC Adv.*, 2017, **7**, 6530–6537.

50 B. Ventura, Y. M. Poronik, I. Deperasińska and D. T. Gryko, *Chem. – Eur. J.*, 2016, **22**, 15380–15388.
51 A. D'Aléo, D. Gachet, V. Heresanu, M. Giorgi and F. Fages, *Chem. – Eur. J.*, 2012, **18**, 12764–12772.
52 S. Li, L. Fu, X. Xiao, H. Geng, Q. Liao, Y. Liao and H. Fu, *Angew. Chem., Int. Ed.*, 2021, **60**, 18059–18064.
53 R. Yoshii, A. Hirose, K. Tanaka and Y. Chujo, *J. Am. Chem. Soc.*, 2014, **136**, 18131–18139.
54 X. Wang, Y. Wu, Q. Liu, Z. Li, H. Yan, C. Ji, J. Duan and Z. Liu, *Chem. Commun.*, 2015, **51**, 784–787.
55 L. Zhou, D. Xu, H. Gao, C. Zhang, F. Ni, W. Zhao, D. Cheng, X. Liu and A. Han, *J. Org. Chem.*, 2016, **81**, 7439–7447.
56 D.-E. Wu, X.-L. Lu and M. Xia, *New J. Chem.*, 2015, **39**, 6465–6473.
57 H. Gao, D. Xu, Y. Wang, C. Zhang, Y. Yang, X. Liu, A. Han and Y. Wang, *Dyes Pigm.*, 2018, **150**, 165–173.
58 T. Butler, W. A. Morris, J. Samonina-Kosicka and C. L. Fraser, *ACS Appl. Mater. Interfaces*, 2016, **8**, 1242–1251.
59 W. A. Morris, T. Butler, M. Kolpaczynska and C. L. Fraser, *Mater. Chem. Front.*, 2017, **1**, 158–166.
60 M. A. Potopnyk, R. Lytvyn, Y. Danyliv, M. Ceborska, O. Bezvikonnyi, D. Volyniuk and J. V. Gražulevicius, *J. Org. Chem.*, 2018, **83**, 1095–1105.
61 K. Benelhadj, J. Massue, P. Retailleau, G. Ulrich and R. Ziessel, *Org. Lett.*, 2013, **15**, 2918–2921.
62 A. Zakrzewska, R. Zalesny, E. Kolehmainen, B. Omiałowski, B. Jedrzejewska, H. Ågren and M. Pietrzak, *Dyes Pigm.*, 2013, **99**, 957–965.
63 B. Osmiałowski, A. Zakrzewska, B. Jedrzejewska, A. Grabarz, R. Zalesny, W. Bartkowiak and E. Kolehmainen, *J. Org. Chem.*, 2015, **80**, 2072–2080.
64 A. M. Grabarz, B. Jedrzejewska, A. Zakrzewska, R. Zalesny, A. D. Laurent, D. Jacquemin and B. Osmiałowski, *J. Org. Chem.*, 2017, **82**, 1529–1537.
65 K. Morokuma, *J. Chem. Phys.*, 1971, **55**, 1236–1244.
66 T. Ziegler and A. Rauk, *Theor. Chim. Acta*, 1977, **46**, 1–10.
67 K. Kitaura and K. Morokuma, *Int. J. Quantum Chem.*, 1976, **10**, 325–340.
68 P. S. Bagus, K. Hermann and C. W. Bauschlicher, *J. Chem. Phys.*, 1984, **80**, 4378.
69 W. J. Stevens and W. H. Fink, *Chem. Phys. Lett.*, 1987, **139**, 15–22.
70 E. D. Glendening and A. Streitwieser, *J. Chem. Phys.*, 1994, **100**, 2900.
71 Y. Mo, J. Gao and S. D. Peyerimhoff, *J. Chem. Phys.*, 2000, **112**, 5530.
72 P. Su and H. Li, *J. Chem. Phys.*, 2009, **131**, 014102.
73 M. Gutowski, F. V. Duijneveldt, G. Chałasiński and L. Piela, *Mol. Phys.*, 1987, **61**, 233–247.
74 W. A. Sokalski, S. Roszak and K. Pecul, *Chem. Phys. Lett.*, 1988, **153**, 153–159.
75 S. M. Cybulski, G. Chałasiński and R. Moszyński, *J. Chem. Phys.*, 1990, **92**, 4357–4363.
76 G. Chałasiński and M. M. Szcześniak, *Chem. Rev.*, 1994, **94**, 1723–1765.
77 G. Chałasiński and M. M. Szcześniak, *Mol. Phys.*, 1988, **63**, 205–224.
78 F. B. van Duijneveldt, J. G. C. M. van Duijneveldt-van de Rijdt and J. H. van Lenthe, *Chem. Rev.*, 1994, **94**, 1873–1885.
79 R. Moszyński, S. Rybak, S. Cybulski and G. Chałasiński, *Chem. Phys. Lett.*, 1990, **166**, 609–614.
80 S. Grimme, *J. Chem. Phys.*, 2003, **118**, 9095–9102.
81 S. F. Boys and F. Bernardi, *Mol. Phys.*, 1970, **19**, 553–566.
82 J.-D. Chai and M. Head-Gordon, *Phys. Chem. Chem. Phys.*, 2008, **10**, 6615–6620.
83 M. J. Frisch, G. W. Trucks, H. B. Schlegel, G. E. Scuseria, M. A. Robb, J. R. Cheeseman, G. Scalmani, V. Barone, G. A. Petersson, H. Nakatsuji, X. Li, M. Caricato, A. V. Marenich, J. Bloino, B. G. Janesko, R. Gomperts, B. Mennucci, H. P. Hratchian, J. V. Ortiz, A. F. Izmaylov, J. L. Sonnenberg, D. Williams-Young, F. Ding, F. Lipparini, F. Egidi, J. Goings, B. Peng, A. Petrone, T. Henderson, D. Ranasinghe, V. G. Zakrzewski, J. Gao, N. Rega, G. Zheng, W. Liang, M. Hada, M. Ehara, K. Toyota, R. Fukuda, J. Hasegawa, M. Ishida, T. Nakajima, Y. Honda, O. Kitao, H. Nakai, T. Vreven, K. Throssell, J. A. Montgomery, Jr., J. E. Peralta, F. Ogliaro, M. J. Bearpark, J. J. Heyd, E. N. Brothers, K. N. Kudin, V. N. Staroverov, T. A. Keith, R. Kobayashi, J. Normand, K. Raghavachari, A. P. Rendell, J. C. Burant, S. S. Iyengar, J. Tomasi, M. Cossi, J. M. Millam, M. Klene, C. Adamo, R. Cammi, J. W. Ochterski, R. L. Martin, K. Morokuma, O. Farkas, J. B. Foresman and D. J. Fox, *Gaussian Revision C.01*, Gaussian Inc., Wallingford CT, 2019.
84 T. H. Dunning, *J. Chem. Phys.*, 1989, **90**, 1007–1023.
85 R. A. Kendall, T. H. Dunning and R. J. Harrison, *J. Chem. Phys.*, 1992, **96**, 6796–6806.
86 D. E. Woon and T. H. Dunning, *J. Chem. Phys.*, 1994, **100**, 2975–2988.
87 M. Feyereisen, G. Fitzgerald and A. Komornicki, *Chem. Phys. Lett.*, 1993, **208**, 359–363.
88 F. Weigend, M. Häser, H. Patzelt and R. Ahlrichs, *Chem. Phys. Lett.*, 1998, **294**, 143–152.
89 F. Weigend, A. Köhn and C. Hättig, *J. Chem. Phys.*, 2002, **116**, 3175–3183.
90 F. Weigend, *Phys. Chem. Chem. Phys.*, 2002, **4**, 4285–4291.
91 H.-J. Werner, F. R. Manby and P. J. Knowles, *J. Chem. Phys.*, 2003, **118**, 8149–8160.
92 M. W. Schmidt, K. K. Baldridge, J. A. Boatz, S. T. Elbert, M. S. Gordon, J. H. Jensen, S. Koseki, N. Matsunaga, K. A. Nguyen, S. Su, T. L. Windus, M. Dupuis and J. A. Montgomery Jr, *J. Comput. Chem.*, 1993, **14**, 1347–1363.
93 R. W. Gora, *EDS package, Revision 2.8.3*, Wrocław, Poland, 1998–2008.
94 H.-J. Werner, P. J. Knowles, G. Knizia, F. R. Manby, M. Schütz, P. Celani, W. Györffy, D. Kats, T. Korona, R. Lindh, A. Mitrushenkov, G. Rauhut, K. R. Shamasundar, T. B. Adler, R. D. Amos, S. J. Bennie, A. Bernhardsson, A. Berning, D. L. Cooper, M. J. O. Deegan, A. J. Dobbyn, F. Eckert, E. Goll, C. Hampel, A. Hesselmann, G. Hetzer, T. Hrenar, G. Jansen, C. Köppl, S. J. R. Lee, Y. Liu, A. W. Lloyd, Q. Ma, R. A. Mata, A. J. May, S. J. McNicholas, W. Meyer, T. F. Miller III, M. E. Mura, A. Nicklass, D. P. O'Neill, P. Palmieri, D. Peng,

K. Pflüger, R. Pitzer, M. Reiher, T. Shiozaki, H. Stoll, A. J. Stone, R. Tarroni, T. Thorsteinsson, M. Wang and M. Welborn, MOLPRO, version 2012.1, a Package of ab initio Programs, 2012, http://www.molpro.net.

95 C. Lee, W. Yang and R. G. Parr, *Phys. Rev. B: Condens. Matter Mater. Phys.*, 1988, **37**, 785–789.

96 V. A. Rassolov, M. A. Ratner, J. A. Pople, P. C. Redfern and L. A. Curtiss, *J. Comput. Chem.*, 2001, **22**, 976–984.

97 A. A. Granovsky, *J. Chem. Phys.*, 2011, **134**, 214113.

98 D. P. Chong, *Recent Advances in Density Functional Methods*, World Scientific, 1995.

99 A. A. Granovsky, Firefly ver. 8, http://classic.chem.msu.su/gran/firefly/index.html.

100 *TURBOMOLE V7.4 2019*, 2019, a development of University of Karlsruhe and Forschungszentrum Karlsruhe GmbH, 1989-2007, TURBOMOLE GmbH, since 2007; available from http://www.turbomole.com.

101 X. Gao, S. Bai, D. Fazzi, T. Niehaus, M. Barbatti and W. Thiel, *J. Chem. Theory Comput.*, 2017, **13**, 515–524.

102 R. R. Valiev, V. N. Cherepanov, G. V. Baryshnikov and D. Sundholm, *Phys. Chem. Chem. Phys.*, 2018, **20**, 6121–6133.

103 R. R. Valiev, V. N. Cherepanov, R. T. Nasibullin, D. Sundholm and T. Kurten, *Phys. Chem. Chem. Phys.*, 2019, **21**, 18495–18500.

104 R. R. Valiev, R. T. Nasibullin, V. N. Cherepanov, G. V. Baryshnikov, D. Sundholm, H. Ågren, B. F. Minaev and T. Kurtén, *Phys. Chem. Chem. Phys.*, 2020, **22**, 22314–22323.

105 R. R. Valiev, R. T. Nasibullin, V. N. Cherepanov, A. Kurtsevich, D. Sundholm and T. Kurtén, *Phys. Chem. Chem. Phys.*, 2021, **23**, 6344–6348.

106 J. Bednarska, R. Zaleny, M. Wielgus, B. Jedrzejewska, R. Puttreddy, K. Rissanen, W. Bartkowiak, H. Ågren and B. Ośmiałowski, *Phys. Chem. Chem. Phys.*, 2017, **19**, 5705–5708.

107 A. Zakrzewska, E. Kolehmainen, A. Valkonen, E. Haapaniemi, K. Rissanen, L. Checińska and B. Omiałowski, *J. Phys. Chem. A*, 2013, **117**, 252–256.

108 G. M. Sheldrick, *Acta Crystallogr.*, 2015, **C71**, 3–8.

109 CrysAlisPro 171.38.43 Package of Programs. Rigaku Oxford Diffraction, 2015.

110 B. Jedrzejewska, A. Grabarz, W. Bartkowiak and B. Omiałowski, *Spectrochim. Acta, Part A*, 2018, **199**, 86–95.

111 V. G. Plotnikov, *Int. J. Quantum Chem.*, 1979, **16**, 527–541.

112 Y. M. Poronik, G. V. Baryshnikov, I. Deperasińska, E. M. Espinoza, J. A. Clark, H. Ågren, D. T. Gryko and V. I. Vullev, *Chem. Commun.*, 2020, **3**, 190.

113 S. M. Cybulski and M. L. Lytle, *J. Chem. Phys.*, 2007, **127**, 141102.

114 B. Kupcewicz and M. Małecka, *Cryst. Growth Des.*, 2015, **15**, 3893–3904.

115 X. He, J. Zhao, Z. Tan, J. Zhao, X. Cheng and C. Zhou, *CrystEngComm*, 2020, **22**, 3110–3114.

116 T. Iwasaki, S. Murakami, Y. Takeda, G. Fukuhara, N. Tohnai, Y. Yakiyama, H. Sakurai and N. Kambe, *Chem. – Eur. J.*, 2019, **25**, 14817–14825.

117 V. S. Padalkar, D. Sakamaki, K. Kuwada, A. Horio, H. Okamoto, N. Tohnai, T. Akutagawa, K.-I. Sakai and S. Seki, *Asian J. Org. Chem.*, 2016, **5**, 938–945.

118 S.-Y. Park, M. Ebihara, Y. Kubota, K. Funabiki and M. Matsui, *Dyes Pigm.*, 2009, **82**, 258–267.

119 K. Yoshida, Y. Ooyama, H. Miyazaki and S. Watanabe, *J. Chem. Soc., Perkin Trans. 2*, 2002, 700–707.

